Novel limiting Criterion for Discontinuous Galerkin Method Applied in Shallow Water Equations

Martin Fišer[1,*],

1 NTIS - New Technologies for the Information Society, Faculty of Applied Sciences, University of West Bohemia, Pilsen, Czech Republic

∗ E-mail: martin.fischer1415@gmail.com

Abstract

This paper presents a novel limiting criterion for discontinuous Galerkin method implemented for shallow water models and the third order accurate schemes. This novel criterion defines 'troubled cells' which have to be limited. In the paper there is also successfully implemented wet/dry interface treatment which ensures non-negativity of the water depth. The limiting criterion uses surface gradient method for water depth limiting. The second order accurate Runge-Kutta method is used for the time integration. The novel method is tested by well-known computational benchmarks for which an analytical solution can be derived.

Keywords

shallow water equations, wet/dry interface, HLL scheme, uneven bed, discontinuous Galerkin method, limiting process, bed slope source term

1 Introduction

Environmental and geophysical flow modeling commonly relies on the numerical solution of the depth-averaged shallow water equations (SWE). While finite volume discretizations with Godunov-type numerical fluxes are currently favored for solving the SWE—see, for example, [15, 18, 21, 29, 33, 40, 47], there has been significant effort put into developing discontinuous Galerkin finite element (DGFEM) discretizations, for example, [11, 12, 24, 26, 34, 44, 45].

Many realistic SWE applications involve wetting and drying processes, for example coastal simulations may involve wave runup and overtopping [32, 44, 45], rainfall-runoff simulations involve very small water depths and cells frequently dry out and get flooded [29,40,46], and urban flood simulations involve advancing wet–dry fronts [18]. The proper numerical treatment of these wet–dry interfaces is directly related to crucial properties, which according to [11] must be satisfied by the numerical scheme in order to ensure an accurate solution. These properties are (i) mass conservation, (ii) C-property, (iii) well-balancedness, (iv) positivity-preserving, and (v) shock-capturing.

In most of these cases wetting and drying processes of the cells occur during the simulation, e.g. part of the computational domain may fall dry or the domain may start initially dry and get flooded. The interface between a wet and a dry cell is usually referred to as a wet/dry interface [5,6]. In [45] the wet/dry interface treatment is described for the second order DGFEM. In this work the treatment suitable for the third order DGFEM is suggested.

The mathematical model of shallow water equations contains the source terms. The bed slope source term is caused by the bed irregularities. This source term is well described in many works like [1, 2, 5, 26, 42].

Except for wet/dry interface and bed slope source term, special treatment is also needed if the shocks and discontinuities are present in the computational domain. High order accuracy schemes have to be limited to prevent them from the appearance of non-physical oscillations. In the theory of the finite volume method with linear reconstruction of the conservative variables, some TVD-minmod limiter restricts the variation of the local slope of the linear approximation with respect to the upstream and downstream gradients. This is referred to as a global limiting process. Accordingly to [27, 37] this global limiting approach leads to the loss of accuracy. Thus the limiter is used only in 'troubled' cells. In [27] the discontinuity detection scheme was used to define these cells. The same criterion was used in [2]. In [26], Kesserwani added the criterion of monotonicity of the solution. Disadvantage of the discontinuity criterion is the definition of the discontinuity itself. Discontinuity in the solution is compared with a predefined constant which defines the 'troubled' cells. Unfortunately this constant can be arbitrarily large and depends on the study case. Within this work we suggest novel criterion of defining 'troubled' cells. This criterion is based on the shape of the solution in the finite element cell and not depends on any constant.

In the 'troubled' cells the limiting process is implemented. In [2, 23], the limiting-dissipation operator was used to limit the numerical solution. Artificial viscosity was used for example in [7, 8, 50]. Within this work, the process described in [13] is used. The solution is limited by decreasing of the order of accuracy to the second order. This second order solution was then limited by minmod limiter. Finite volume limiters were also adopted in [48].

The novel criterion of defining 'troubled' cells and wet/dry interface treatment are tested and validated by the classical benchmarks and compared by other numerical methods and analytical solutions at the end of this paper.

2 Governing Equations

Depth-averaged one-dimensional shallow water equations can be written in conservative form as

$$\frac{\partial \mathbf{W}}{\partial t} + \frac{\partial \mathbf{F}}{\partial x} = \mathbf{S}_b, \tag{1}$$

where $\mathbf{W}$ is the vector of conservative variables described by the water depth h and flow velocity u as

$$\mathbf{W} = \begin{bmatrix} h \\ hu \end{bmatrix}, \tag{2}$$

$\mathbf{F}$ is the vector function of inviscid flux

$$\mathbf{F} = \begin{bmatrix} hu \\ hu^2 + \frac{1}{2}gh^2 \end{bmatrix}, \tag{3}$$

here g is gravity acceleration. Bed slope source term $\mathbf{S}_b$ is defined as

$$\mathbf{S}_b = \begin{bmatrix} 0 \\ -gh\frac{\partial B(x)}{\partial x} \end{bmatrix}, \tag{4}$$

where $B(x)$ is the bottom topography. $B(x)$ might vary in time, however is considered time-independent in this work.

The source vector may further contain rain source term, bed friction term, fluid viscosity effects, wind shear, turbulent viscosity or Coriolis forces, depending on the case under consideration. These effects are neglected in this work.

3 Numerical Scheme of Discontinuous Galerkin Method

In this section, numerical scheme of DGFEM is describe. However, it is only basic description of the method. More detailed description of the method can be found in [38].

If not redefined, the following nomenclature is used in the article. Index k is iterator over the equations in the mathematical model (i.e., k varies from 1 to 2 in case of 1D SWE model). Index i is iterator over the finite elements. Index p iterates over the Gaussian points and indexes j and l iterate over the basis functions.

Let us consider a 1D computational area $\Omega = [a, b] \subset \mathbb{R}$ and let $t \in [0, T]$. Let $\mathcal{T} = \{\Omega_i\}_{i=1}^{n}$ be the discretization of the computational area where $\Omega_i = [x_{i-\frac{1}{2}}, x_{i+\frac{1}{2}}]$ and $\cup_i \Omega_i = \Omega$.

The solution of (1) is from the space $\mathbf{S}_h = S_h \oplus S_h$ such that

$$S_h = \{q \in L^2([a, b]) : q|_{\Omega_i} \in P^p(\Omega_i), \forall \Omega_i\} \tag{5}$$

here $P^p(\Omega_i)$ is the space of polynomials with degree less than or equal to p in Ω_i. The set $\{\varphi_i^j\}_{j=1}^{n_b}$ is a basis of the space $P^p(\Omega_i)$.

The multiplying of the Equation 1 by the testing function $\mathbf{v}(x) \in \mathbf{S}_h$ and integrating over the finite element Ω_i yields

$$\int_{\Omega_i} \frac{\partial \mathbf{W}(x,t)}{\partial t} \cdot \mathbf{v}(x)\ d\Omega + \int_{\Omega_i} \frac{\partial \mathbf{F}(x,t)}{\partial x} \cdot \mathbf{v}(x)\ d\Omega = \int_{\Omega_i} \mathbf{S}(x,t) \cdot \mathbf{v}(x)\ d\Omega, \tag{6}$$

where '$\cdot$' means scalar product. The second integral can be modified in aid of integration-

by-parts

$$\int_{\Omega_i} \frac{\partial \mathbf{W}(x,t)}{\partial t}\mathbf{v}(x)\ d\Omega + \oint_{\partial\Omega_i} \mathbf{F}(x,t)\mathbf{v}(x)\vec{n}\ ds - \int_{\Omega_i} \mathbf{F}(x,t)\frac{\partial v(x)}{\partial x}\ d\Omega = \int_{\Omega_i} \mathbf{S}(x,t)v(x)\ d\Omega, \tag{7}$$

where $\partial\Omega_i$ is the boundary of the cell Ω_i and $\vec{n}$ is an outer normal vector. Provided that in 1D case the computational cell is an interval $\Omega_i = [x_{i-\frac{1}{2}}, x_{i+\frac{1}{2}}]$, the curve integral $\oint_{\partial\Omega_i} \mathbf{F}(x,t)\mathbf{v}(x)\vec{n}\ ds$ can be replaced by the values at the edges

$$\oint_{\partial\Omega_i} \mathbf{F}(x,t)\mathbf{v}(x)\vec{n}\ ds = [\mathbf{F}(x,t)\mathbf{v}(x)]_{x-\frac{1}{2}}^{x+\frac{1}{2}} = \mathbf{F}(x_{i+\frac{1}{2}},t)\mathbf{v}(x_{i+\frac{1}{2}}) - \mathbf{F}(x_{i-\frac{1}{2}},t)\mathbf{v}(x_{i-\frac{1}{2}}). \tag{8}$$

In general case, the solution at the edge of the finite element can be discontinuous, thus the flux $\mathbf{F}$ must be replaced by numerical flux Φ at this place. The numerical flux can be computed by some Riemann solver such as Lax-Friedrich flux [30], Roe scheme [39] or AUSM scheme [31]. In this work, HLL scheme proposed in [19] is used. This scheme is based on the estimation of the largest and the smallest discontinuities propagation speeds. This speeds can be estimated by eigenvalues of the system (1)

$$\begin{aligned} a^-_{i+\frac{1}{2}} &= min\left\{\lambda_1\left(\mathbf{W}_L\right), \lambda_1\left(\mathbf{W}_R\right), 0\right\}, \\ a^+_{i+\frac{1}{2}} &= max\left\{\lambda_2\left(\mathbf{W}_L\right), \lambda_2\left(\mathbf{W}_R\right), 0\right\}, \end{aligned} \tag{9}$$

where $W_{L/R}$ stands for the values of the conservative variable vector on the left and right side of an edge. Eigenvalues λ_1, λ_2 are defined as

$$\begin{aligned} \lambda_1 &= u - \sqrt{gh}, \\ \lambda_2 &= u + \sqrt{gh}. \end{aligned} \tag{10}$$

The final numerical flux is computed as

$$\mathbf{\Phi} = \frac{a^+_{i+\frac{1}{2}}\mathbf{F}\left(\mathbf{W}_L\right) - a^-_{i+\frac{1}{2}}\mathbf{F}\left(\mathbf{W}_R\right)}{a^+_{i+\frac{1}{2}} - a^-_{i+\frac{1}{2}}} + \frac{a^+_{i+\frac{1}{2}}a^-_{i+\frac{1}{2}}}{a^+_{i+\frac{1}{2}} - a^-_{i+\frac{1}{2}}}\left[\mathbf{W}_R - \mathbf{W}_L\right]. \tag{11}$$

The components of the solution $\mathbf{W}_i = [W_{i,1}, W_{i,2}]^T = [h_i, (hu)_i]^T$ are described by the linear combination of the spatial dependant basis functions $\varphi_i(x)$ and time dependant coefficients $w_{i,k}(t)$ as

$$W_{i,k}(x,t) = \sum_{j=1}^{n_b} w^j_{i,k}(t)\varphi^j_i(x), \quad k = 1, 2, \tag{12}$$

here $W_{i,k}(x,t)$ is conservative variable (water depth h for k=1 and discharge hu for k=2) and n_b is number of the basis functions. For the sake of simplicity the parameters of the functions will be omitted in the following.

Let us take the testing function $\mathbf{v}(x) = v_{i,k}(x),\ k = 1, 2$, where

$$\mathbf{v}_{i,1} = \begin{bmatrix} \varphi^l_i(x) \\ 0 \end{bmatrix} \tag{13}$$

and

$$\mathbf{v}_{i,2} = \begin{bmatrix} 0 \\ \varphi^l_i(x) \end{bmatrix} \tag{14}$$

For the sake of simplicity the parameters of the functions will be omitted in the following. Substitution of (12) into (7) results in the system of differential equations

$$\sum_{j=1}^{n_b} \frac{\mathrm{d}w^j_{i,k}}{\mathrm{d}t} \int_{\Omega_i} \varphi^j_i \varphi^l_i \, d\Omega + \left[\Phi_k \varphi^l_i\right]_{x-\frac{1}{2}}^{x+\frac{1}{2}} - \int_{\Omega_i} F_k \frac{\partial \varphi^l_i}{\partial x} \, d\Omega = \int_{\Omega_i} S_{Bk} \varphi^l_i \, d\Omega,\ l = 1, 2, \dots, n_b \tag{15}$$

where F_k, Φ_k or S_{Bk} means the k^{th} component of inviscid flux (3), numerical flux (11) or bed slope source term (4) respectively. The system of equations (15) can be expressed in compact vector form as

$$\mathbf{M}_i \frac{\mathrm{d}}{\mathrm{d}t}\mathbf{w}_{i,k} = \mathbf{RHS}_{i,k} \tag{16}$$

where local mass matrix $\mathbf{M}_i$ is computed as

$$\mathbf{M}_i = \int_{\Omega_i} \varphi_i^l \varphi_i^j \, d\Omega, \tag{17}$$

$\mathbf{w}_{i,k} = [w_{i,k}^1, w_{i,k}^2, \ldots, w_{i,k}^{n_b}]^T$ is vector of time dependent coefficients and vector $\mathbf{RHS}_{i,k}$ is created by the components

$$RHS_{i,k}^l = -\oint_{\partial\Omega_i} \Phi_k \varphi_i^l \, ds + \int_{\Omega_i} F_k \frac{\partial \varphi_i^l}{\partial x} \, d\Omega + \int_{\Omega_i} S_{Bi,k} \varphi_i^l \, d\Omega, \quad l = 1, 2, \ldots, n_b. \tag{18}$$

The time integration of the semi-discrete scheme

$$\frac{\mathrm{d}}{\mathrm{d}t}\mathbf{w}_{i,k} = \mathbf{M}_i^{-1}\mathbf{RHS}_{i,k} \tag{19}$$

can be done for example by the second order Runge-Kutta method.

4 Novel Limiting Criterion and Limiting Process

Like other high-order methods, DGFEM needs to be limited around the shocks to avoid instability of the scheme.

In case of solution described by the first order polynomials (i.e. linear functions), the limiting method can be done by global limiting process and minmod limiter can be used to decide if the solution should be limited. However, this method cannot be used in case

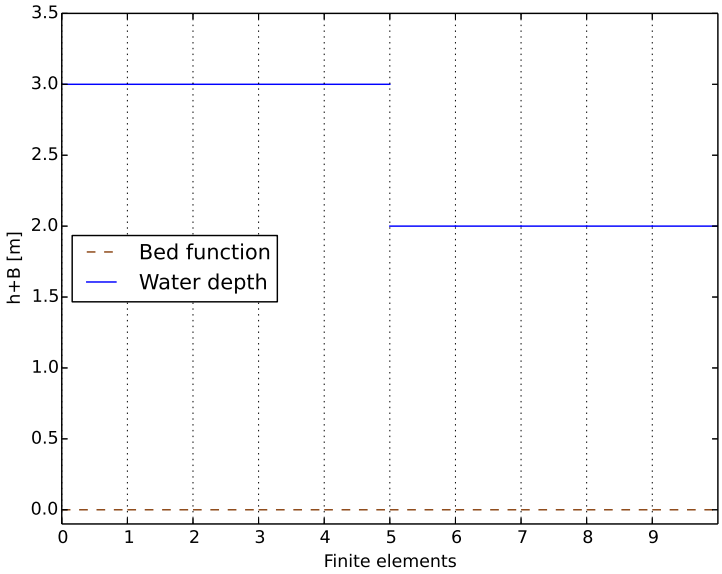

Figure 1: Initial conditions of the Riemann problem.

of the second order polynomials as the slope of the solution cannot be easily compared by the upwind and downwind differences

$$\delta^- W_{i,k} = \frac{W_{i,k} - W_{i-1,k}}{\Delta x}, \quad \delta^+ W_{i,k} = \frac{W_{i+1,k} - W_{i,k}}{\Delta x}, \tag{20}$$

which are used in minmod limiter. Here Δx means the distance between the middles of the adjacent finite volumes.

The initial conditions of the classical Riemann problem can bee seen in Figure 1 where the water depth and flat bed function is plotted. The initial velocity is zero. It is very likely that non-limited solution around the shock is not monotone and concave or convex as shown for water depth and discharge in Figures 2 and 3. The novel criterion for the second order polynomial base functions suppose, that the solution in the centre of the finite element must be bounded by the values at the edge of this element. If the solution

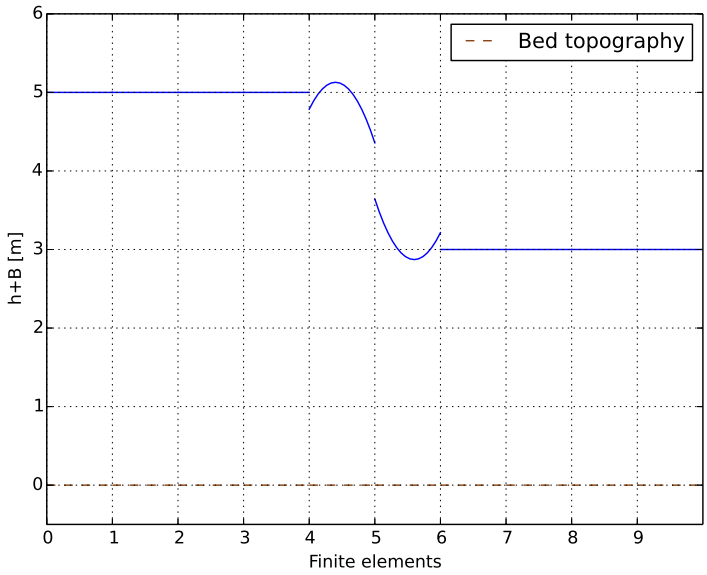

Figure 2: First time iteration of non-limited water depth.

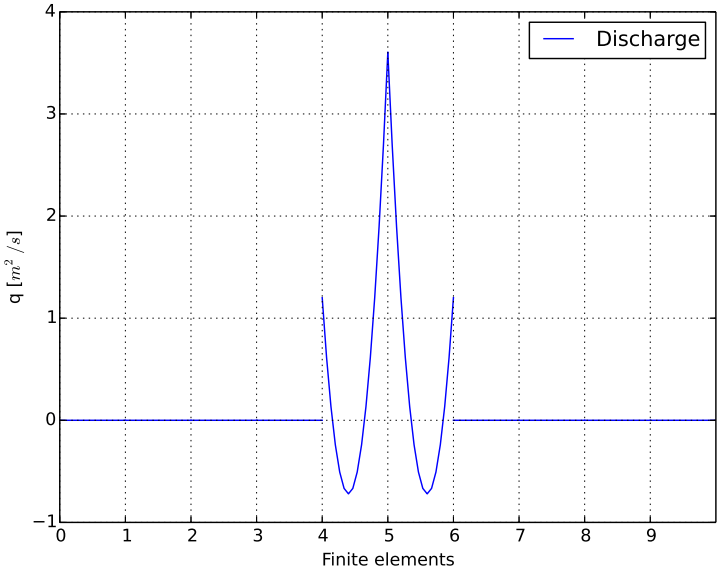

Figure 3: First time iteration of non-limited discharge.

Table 1: Legendre polynomials

Base function	Legendre polynomial
φ^1	1
φ^2	x
φ^3	$\frac{1}{2}(3x^2-1)$

in the middle is not bounded, i.e.

$$\begin{gathered} min\left(W_{i,k}(x_{i-\frac{1}{2}},t),W_{i,k}(x_{i+\frac{1}{2}},t\right) > W_{i,k}(x_i,t) \\ \text{or} \\ max\left(W_{i,k}(x_{i-\frac{1}{2}},t),W_{i,k}(x_{i+\frac{1}{2}},t)\right) < W_{i,k}(x_i,t) \end{gathered} \tag{21}$$

the cell is defined as 'troubled' and the solution of a conservative variable must be limited in this cell.

The solution in the 'troubled' cells must be limited. The limiting process, used within this work, is similar to the limiting process of Cockburn and Shu [13]. This process consist in lowering the polynomial order and employing suitable limiter. As a basis functions the Legendre polynomials are used.

This polynomials can bee seen in Table 1. Let us consider the range of these polynomials $[-1,1]$. Interval $[-1,1]$ can be mapped to the arbitrary interval $[x_{i-\frac{1}{2}},x_{i+\frac{1}{2}}]$ by linear transformation (linear mapping)

$$x = x_{i-\frac{1}{2}}\frac{1-\xi}{2} + x_{i+\frac{1}{2}}\frac{1+\xi}{2}, \quad x\in[x_{i-\frac{1}{2}},x_{i+\frac{1}{2}}], \quad \xi\in[-1,1]. \tag{22}$$

Legendre polynomials are orthogonal in 'integral average' norm, i.e.

$$\int_{-1}^{1}\varphi^j\varphi^l dx \begin{cases} = 0 \text{ for } i\neq j \\ \neq 0 \text{ for } i=j \end{cases} \tag{23}$$

thus the integral averages of φ^2 and φ^3 are zero[1] itself and the scheme is still mass and momentum conservative even if the third coefficient $w^3_{i,k}$ from (12) is set to be zero.

Within this work, the minmod limited was chosen to modify the second coefficient

$$w^2_{i,k} = minmod(\delta^- W_{i,k}, \delta^+ W_{i,k}) \tag{24}$$

where upwind and downwind differences $\delta^{\mp} W_{i,k}$ are defined by (20) and *minmod* function is defined as [35]

$$\text{minmod}(z_1, z_2) = \frac{1}{2}[\text{sgn}(z_1) + \text{sgn}(z_2)] \cdot \min(|z_1|, |z_2|). \tag{25}$$

4.1 Implementation of the Surface Gradient Method

In [49], the Surface Gradient Method (SGM) was introduced. This method has been developed for reconstruction of the water level within the shallow water equations with bed slope source terms. In contrast to conventional data reconstruction methods based on water depth (h) the water surface level ($h + B$) is chosen as the basis for data reconstruction. This provides accurate values of the conservative variables at cell interfaces so that the fluxes can be accurately calculated with a Riemann solver.

If the SGS method is adopted, the 'troubled' cell criterion (21) is defined as

$$\begin{gathered} min\left(W_{i,1}(x_{i-\frac{1}{2}}, t) + B(x_{i-\frac{1}{2}}), W_{i,1}(x_{i+\frac{1}{2}}, t) + B(x_{i+\frac{1}{2}})\right) > W_{i,1}(x_i, t) + B(x_i) \\ \text{or} \\ max\left(W_{i,1}(x_{i-\frac{1}{2}}, t) + B(x_{i-\frac{1}{2}}), W_{i,1}(x_{i+\frac{1}{2}}, t) + B(x_{i+\frac{1}{2}})\right) < W_{i,1}(x_i, t) + B(x_i) \end{gathered} \tag{26}$$

[1]The integral averages of higher Legendre functions are zero because of the orthogonality with the first one $\int_{-1}^{1} \varphi^j \cdot \underbrace{1}_{\varphi^1}\, dx = 0,\ j = 2, 3.$

The limiting process is similar to the process described earlier. The third coefficient $w_{i,1}^3$ is set to zero. The difference is in computation of the second coefficient $w_{i,1}^2$. Upwind and downwind differences used in the limiter (25) are computed as

$$\delta^- W_{i,1} = \frac{(W_{i,1} + B_i) - (W_{i-1,1} + B_{i-1})}{\Delta x}, \quad \delta^+ W_{i,1} = \frac{(W_{i+1,1} + B_{i+1}) - (W_{i,1} + B_i)}{\Delta x}. \tag{27}$$

As in the vector of the conservative variable (2), the water depth (instead of the water level) is stored, the second coefficient must be computed as

$$w_{i,1}^2 = minmod(\delta^- W_{i,1}, \delta^+ W_{i,1}) - \delta B_i \tag{28}$$

where δB_i means the slope of the bed function computed as

$$\delta B_i = \frac{B_{i+\frac{1}{2}} - B_{i-\frac{1}{2}}}{\Delta x_i}. \tag{29}$$

Provided that the piece-wise linear bed function is also described by the linear combination of the bed function coefficients w_i^j and the first two Legendre polynomials

$$B_i(x) = w_{b_i}^1 \cdot 1 + w_{b_i}^2 \cdot x, \tag{30}$$

δB_i is identical to the coefficient w_i^2. Index b implicates that the w_{b_i} coefficients belong to the description of the bed function.

5 Wet/dry Interface

The numerical solvers can yield spurious negative water depth. This non-physical phenomena can occur mainly during the wetting and drying processes in the computational domain as shown in Figure 6. This phenomena is well known from the theory of finite volumes [3, 4, 9, 10, 16, 21, 22, 25, 32]. In [28], Kurganov et al. suggested positivity preserving scheme based on finite volume method. This scheme modifies the slope of linear reconstruction so that there is no negative water depth within the finite volume.

An exemplary finite volume reconstruction resulting in negative water depth at the edge $i - \frac{1}{2}$ is shown in Figure 4. The negative water depth $h_{i-\frac{1}{2}}$ at the edge $i - \frac{1}{2}$ is set to zero and the water depth $h_{i+\frac{1}{2}}$ is computed in such way that the water depth at cell center h_i remains unchanged:

$$\begin{gathered} \underbrace{0}_{h_{i-\frac{1}{2}}} + B_{i-\frac{1}{2}} + \delta h_i \frac{\Delta x_i}{2} = h_i + \frac{B_{i+\frac{1}{2}} + B_{i-\frac{1}{2}}}{2} \\ \Downarrow \\ \delta h_i = \frac{2h_i + B_{i+\frac{1}{2}} - B_{i-\frac{1}{2}}}{\Delta x_i} \end{gathered} \tag{31}$$

Here δh_i is the slope of the water level. Then

$$h_{i+\frac{1}{2}} = h_i + \frac{B_{i+\frac{1}{2}} + B_{i-\frac{1}{2}}}{2} + \delta h_i \frac{\Delta x_i}{2} - B_{i+\frac{1}{2}} = 2h_i. \tag{32}$$

The corrected reconstruction of the water depth is shown in Figure 5. The case when $h_{i+\frac{1}{2}} < 0$ can be corrected in a similar way and the conditions of the correction can be

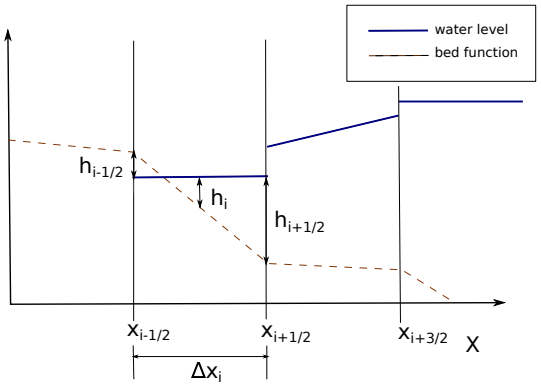

Figure 4: Linear reconstruction of the water depth with the negative water depth $h_{i-\frac{1}{2}}$.

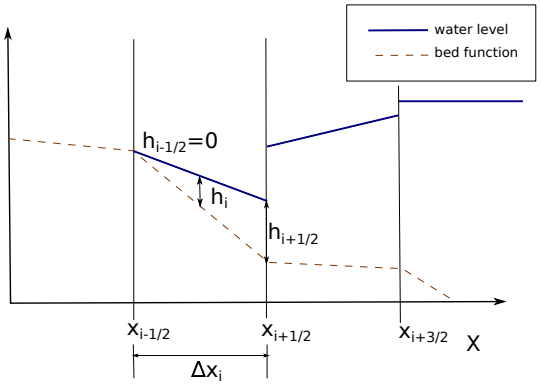

Figure 5: Corrected linear reconstruction of the water depth.

summarized as [28]

$$\text{if} \quad h_{i-\frac{1}{2}} < 0 \begin{cases} h_{i-\frac{1}{2}} = 0 \\ h_{i+\frac{1}{2}} = 2h_i \end{cases}, \qquad \text{if} \quad h_{i+\frac{1}{2}} < 0 \begin{cases} h_{i-\frac{1}{2}} = 2h_i \\ h_{i+\frac{1}{2}} = 0 \end{cases}. \tag{33}$$

After this modification, the non-negativity of the water depth is ensured.

Higher order DGFEM method can produce the negative values of the water depth not only at the edges but also within the finite element as shown in Figure 6. It is computationally demanding to check whole solution within the finite element thus we suggest to check the positivity of the solution only in the points which are used for the computations. These points are the Gaussian points and values at the edges of the finite element. This process results in novel criterion for wet/dry interface. The solution must be limited if

$$W_{i,1}(x_p) < 0 \tag{34}$$

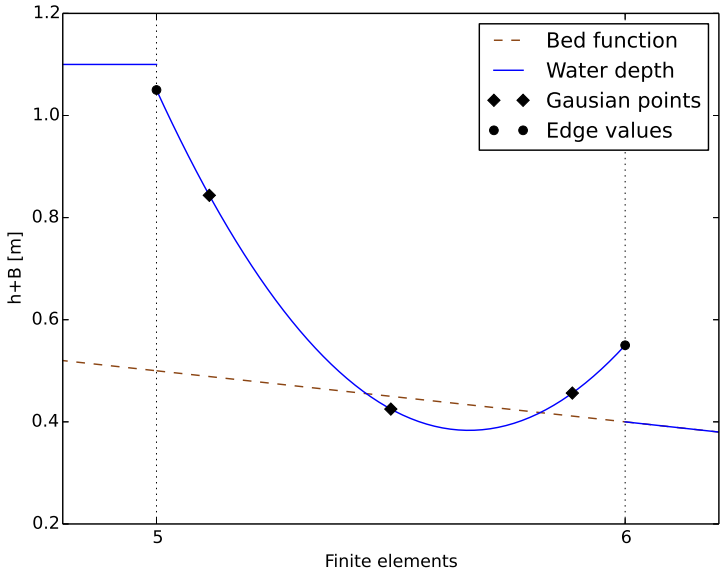

Figure 6: Non-physical solution with negative water depth.

where x_p stands for Gaussian points and points at the edges of the finite element. First part of the limitation of the water depth is similar to that one described in Section 4. The third coefficient is set to be zero which yields the situation depicted in Figure 7. After that, the coefficient $w^2_{i,1}$, governing the slope of the linear function, is altered to gain the same values as in (33). It means that, in case when the water depth $W_{i,1}(x_{i-\frac{1}{2}})$ is negative, the slope of the function can be computed as

$$w^2_{i,1} = \frac{W_{i,1}(x_i) - 0}{\frac{\Delta x_i}{2}} = W_{i,1}(x_i). \tag{35}$$

Let us highlight that $\Delta x_i = 2$ because of the mapping (22) and after the limitation to the linear function, the value of the water depth in the middle of the finite element is equal to the first coefficient, i.e.

$$W_{i,1}(x_i) = w^1_{i,1}. \tag{36}$$

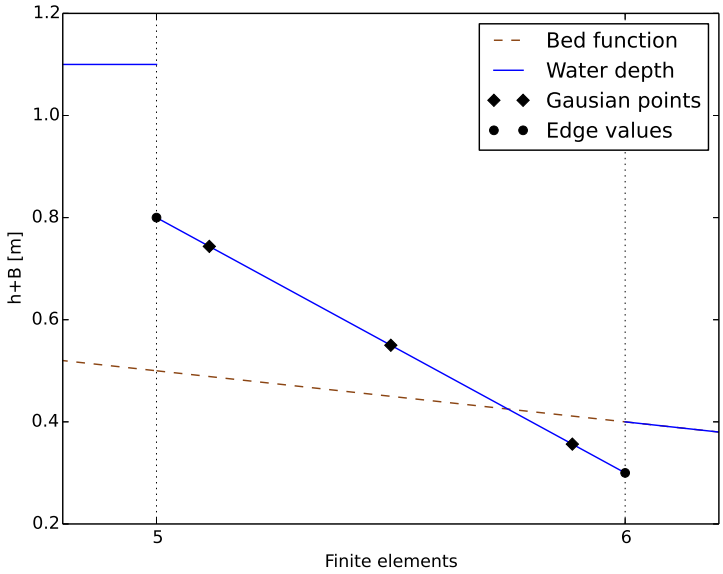

Figure 7: Limited solution of the water depth.

Taking in account (36), relation (35) can be generalised for both edges as

$$w_{i,1}^2 = \begin{cases} w_{i,1}^1, \text{ if } W_{i,1}(x_{i-\frac{1}{2}}) < 0 \\ -w_{i,1}^1, \text{ if } W_{i,1}(x_{i+\frac{1}{2}}) < 0 \end{cases} . \tag{37}$$

Final limited and corrected solution can be seen in Figure 8.

However this water depth may become very small and cause problems with the computation of the velocity u which is computed by the fraction of the discharge (hu) and water depth h

$$u = \frac{(hu)}{h}. \tag{38}$$

Obviously $u \to \infty$ for $h \to 0$. To avoid unrealistic velocities, Kurganov and Petrova [28]

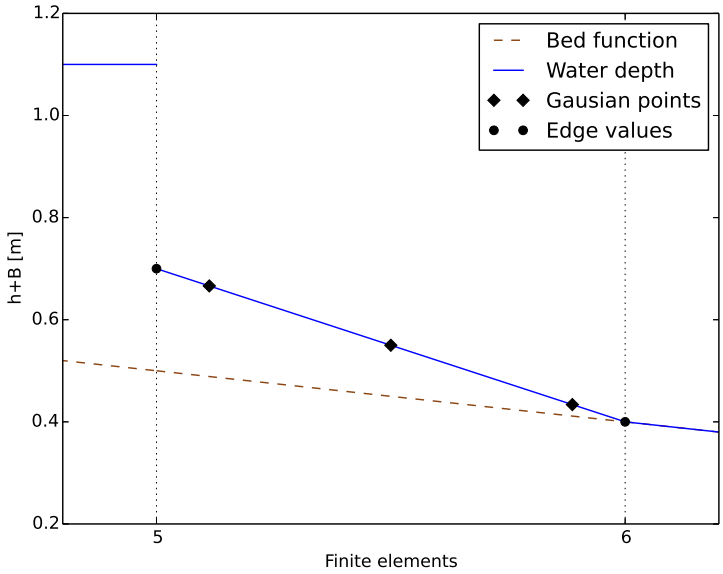

Figure 8: Corrected solution of the water depth.

proposed the following formulae which avoids the division by very small numbers

$$u = \frac{\sqrt{2}h(hu)}{\sqrt{h^4 + \max(h, \epsilon_h)}}. \tag{39}$$

ϵ_h is a small positive constant. In [28] it is recommended to set this constant to $\epsilon_h = (\Delta x_i)^4$. The discharge hu, used in the Riemann solver, has to be recomputed as

$$hu = h \cdot u. \tag{40}$$

6 Numerical Results

In this section, the novel scheme is validated against analytical solutions and compared with other schemes.

6.1 Dam Break on a Wet Domain without Friction

This benchmark is a classical Riemann problem which can be represented by a dam separating two basins with different water depths. The dam is instantaneously removed and the flow patterns are simulated. The analytical solution was firstly introduced in [41]. Simple overview of this solution can be also found in [14]. The initial conditions of the water depth within our simulation are

$$h(x) = \begin{cases} h_l, \text{ for } 0 < x < x_0 \\ h_r, \text{ for } x_0 < x < L \end{cases} \tag{41}$$

where $h_l = 5$ m, $h_r = 3$ m, the position of the dam is $x_0 = 5$ m and the length of the computational domain is $L = 10$ m. The computation is stopped at the time $t = 0.5$ s and compared with the DGFEM global limiting scheme (DGFEM GL) where the minmod limiter was used for the shock detection. The solution of the water level can be seen in Figure 9. This figure shows the results computed by ten finite elements. The convergence of a scheme for given test case can be found by the slope of the $log(L_2\text{error})$ dependent on $log(n_t)$. This slope can bee seen in Figure 10. L_2 error was computed as

$$L_2 \text{ error} = \sqrt{\frac{\sum_{i=1}^{n_t}(h_n(x_i) - h_a(x_i))^2 \Delta x_i}{L}} \tag{42}$$

where x_i are middle points of the finite elements, Δx_i is cell width and h_n/h_a means the numerical/analytical solution. The slopes of the convergence in Figure 10 were computed by the linear regression of L_2 errors. Numerical results shown that the novel scheme gives better accuracy and convergence of the DGFEM.

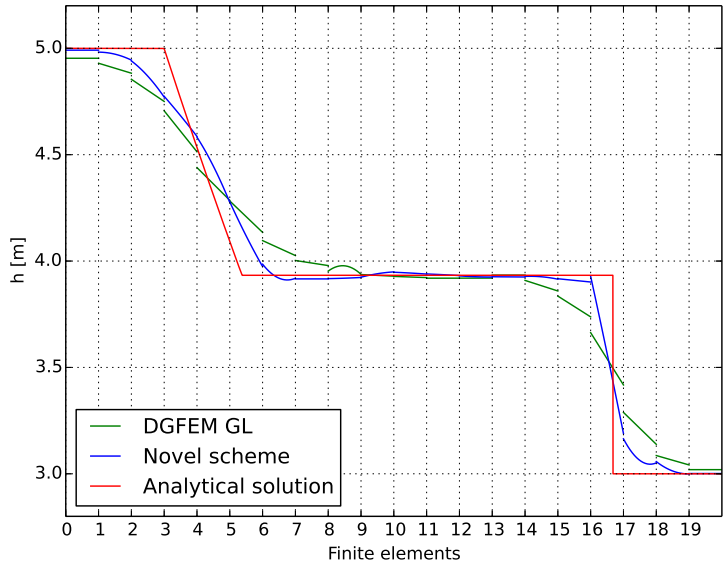

Figure 9: Simulation of the water level. Comparison of the global limiting and novel scheme.

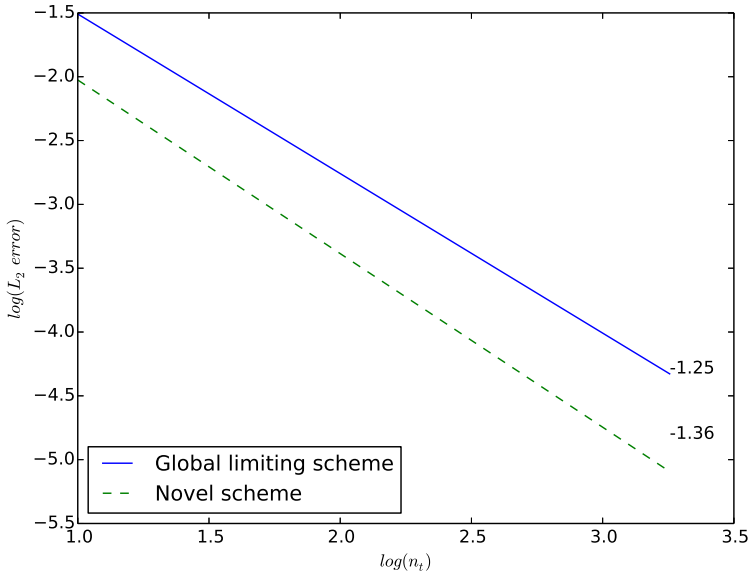

Figure 10: L_2 error convergence of the global limiting and novel scheme.

6.2 Planar surface flow in a parabola

Another benchmark is the planar surface in a parabola without friction. In this bench mark the the wetting and drying processes occur. Two-dimensional exact solution was derived in [43]. Here, one-dimensional simplification presented in [14] is computed. The topography is a parabolic shape given by

$$B(x) = h_0 \left(\frac{1}{a^2} \left(x - \frac{\mathrm{L}}{2} \right)^2 - 1 \right). \tag{43}$$

The analytical solution of the water depth is

$$h(x) = \begin{cases} -h_0 \left(\left(\frac{1}{a} \left(x - \frac{\mathrm{L}}{2} \right) + \frac{C}{\sqrt{2gh_0}} \cos\left(\frac{\sqrt{2gh_0}}{a} t \right) \right)^2 - 1 \right) & \text{for } x_1(t) \leq x \leq x_2(t), \\ 0 \quad \text{otherwise,} \end{cases} \tag{44}$$

with location of the wet/dry interfaces at time t being calculated as

$$\begin{aligned} x_1(t) &= -\tfrac{1}{2} \cos\left(\tfrac{\sqrt{2gh_0}}{a} t \right) - a + \tfrac{\mathrm{L}}{2}, \\ x_2(t) &= -\tfrac{1}{2} \cos\left(\tfrac{\sqrt{2gh_0}}{a} t \right) + a + \tfrac{\mathrm{L}}{2} \end{aligned} \tag{45}$$

and

$$C = \sqrt{\frac{2gh_0}{2a}}. \tag{46}$$

Initial conditions of the water depth are given by (44) for $t = 0$ s and the flow velocity is zero.

In the simulation the following parameters were used: $a = 1$ m, $h_0 = 0.5$ m and $L = 4$ m. Comparison of the simulations and analytical solution was done in time $T = 5\frac{a\pi}{\sqrt{2gh_0}}$. For the comparison L_2 error (42) was used. Novel scheme is compared by the second

order accurate DGFEM scheme. Within second order accurate scheme, the solution is described by the linear function, thus minmod limiter and global limiting method was used for the limiting of the solution. Moreover the scheme was compared with the finite volume scheme with linear reconstruction presented in [17]. Visual comparison with the exact solution, for different numbers of finite elements/volumes, can be seen in Figures 11, 12, 13 and 14. L_2 error convergence is shown in Figure 15.

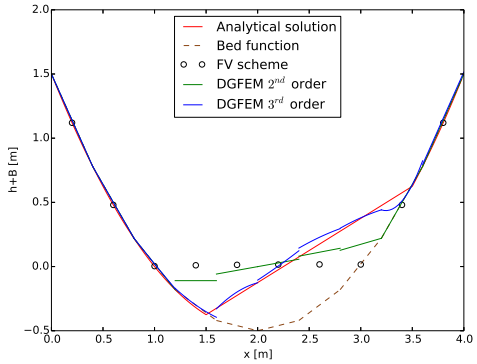

Figure 11: Analytical solution compared with the novel and reference scheme-10 finite elements/volumes.

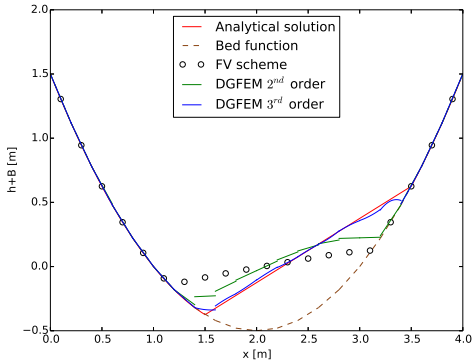

Figure 12: Analytical solution compared with the novel and reference scheme-20 finite elements/volumes.

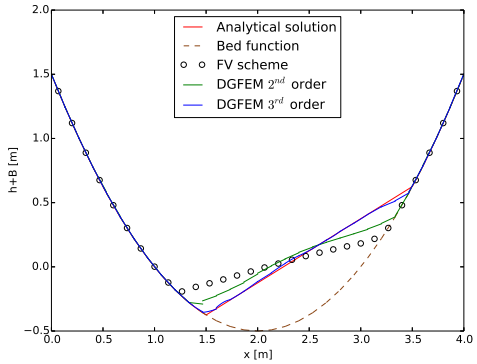

Figure 13: Analytical solution compared with the novel and reference scheme-30 finite elements/volumes.

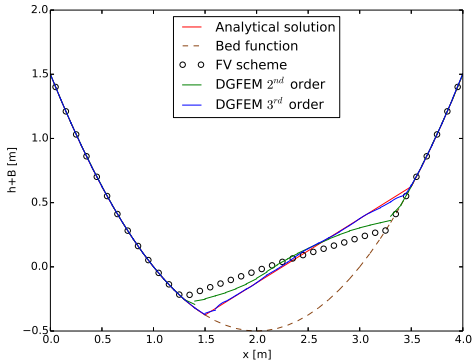

Figure 14: Analytical solution compared with the novel and reference scheme-40 finite elements/volumes.

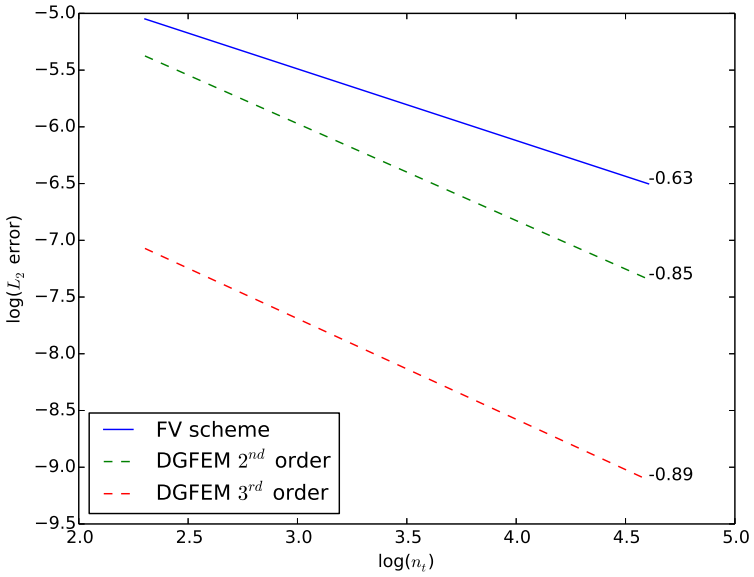

Figure 15: L_2 error convergence of the reference FV scheme and novel DGFEM scheme.

6.3 Flow over the Bump

Another testing benchmark is steady state flow over the bump. The length of the computational domain is L=25 m with a topography given by

$$B(x) = \begin{cases} 0.2 - 0.05(x-10)^2 & \text{if } 8 \text{ m} < x < 12 \text{ m}, \\ 0 & \text{else.} \end{cases} \tag{47}$$

In the following, the numerical results of subcritical flow, transcritical flow and transcritical flow with the shock are shown. The results were computed for coarse mesh created by 20 finite elements. The inlet is set on the left side of the computational domain and the outlet is set on the right side of the computational domain. Initial conditions for all

these three types of flow are

$$\begin{aligned} h(x) + B(x) &= 2, \quad x \in \Omega, \\ u(x) &= 0, \qquad\quad x \in \Omega. \end{aligned} \tag{48}$$

Analytical solutions of steady state flows over the bump can be found for example in [14] or [20]. Novel limiting method was also compared with the global limiting method where the minmod limiter was used for the location of the shock.

The boundary conditions of the subcritical flow are

$$\begin{aligned} q_{inlet} &= 4.42 \ m^2/s \\ h_{outlet} &= 2 \ m \end{aligned} \tag{49}$$

and the water depth is given by the resolution of

$$h^3(x) + \left(B(x) - \frac{q_{inlet}^2}{2gh_{outlet}^2} - h_{outlet} \right) h^2(x) + \frac{q_{inlet}}{2g} = 0, \quad \forall x \in [0, L] \tag{50}$$

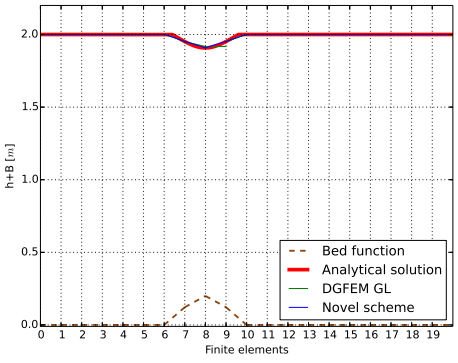

Figure 16: Water depth: subcritical flow.

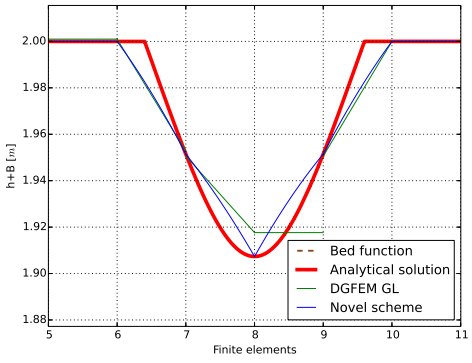

Figure 17: Detail of the water depth: subcritical flow.

The water depth is shown in Figure 16 and in Figure 18 the discharge is shown. Details

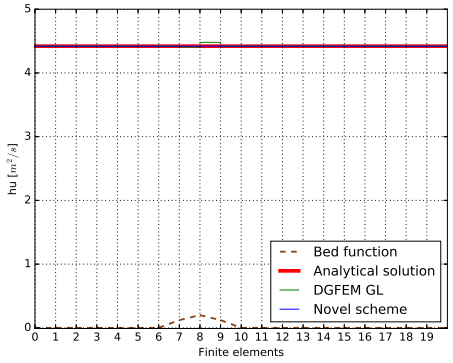

Figure 18: Discharge: subcritical flow.

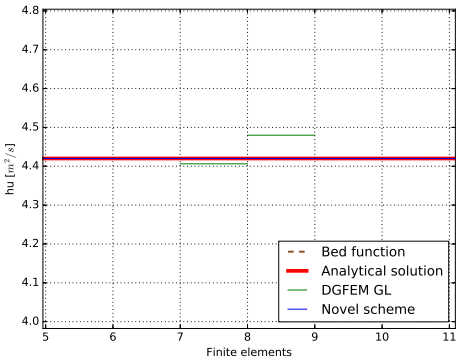

Figure 19: Detail of the discharge: subcritical flow.

of the water depth and discharge can be seen in Figures 17 and 19.

The boundary conditions of the transcritical flow without shock are

$$\begin{aligned} q_{inlet} &= 1.53\ m^2/s, \\ h_{outlet} &= 0.66\ m \end{aligned} \tag{51}$$

and the analytical solution is given by the resolution of

$$h^3(x) + \left(B(x) - \frac{\mathrm{q}_{inlet}^2}{2g\mathrm{h}_M^2} - h_M - B_M \right) h^2(x) + \frac{\mathrm{q}_{inlet}^2}{2g} = 0, \quad \forall x \in [0, L] \tag{52}$$

where $B_M = \max_{x\in[0,L]} B(x)$ and h_M is the corresponding water depth. In Figures 20 and 21 the water depth can be seen and the discharge can be seen in Figures 22 and 23.

Boundary conditions of the transcritical flow with shock are given by

$$\begin{aligned} q_{inlet} &= 0.18\ m^2/s, \\ h_{outlet} &= 0.33\ m. \end{aligned} \tag{53}$$

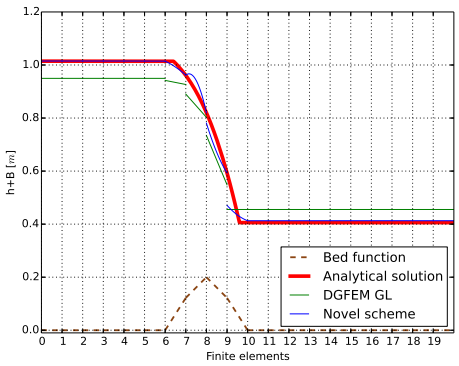

Figure 20: Water depth: transcritical flow without the shock.

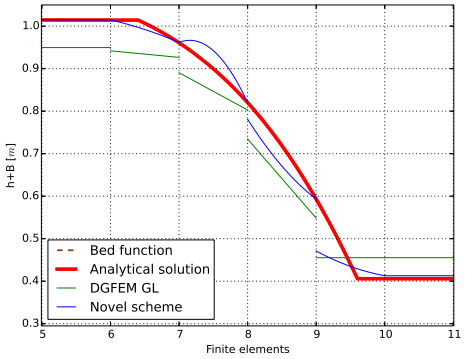

Figure 21: Detail of the water depth: transcritical flow without the shock.

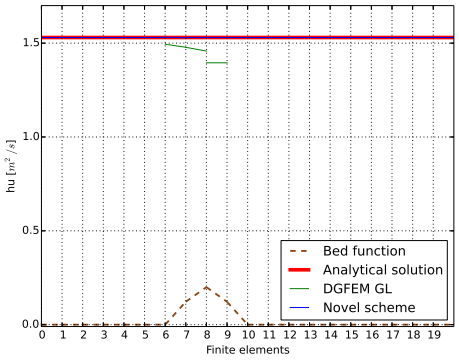

Figure 22: Discharge: transcritical flow without the shock.

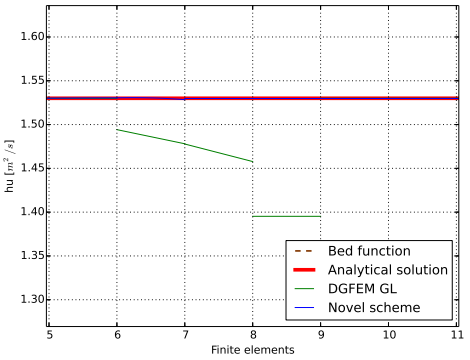

Figure 23: Detail of the discharge: transcritical flow without the shock.

and the analytical solution is given by the resolution of

$$\begin{aligned} h^3(x_{shock}) + \left(B(x_{shock}) - \frac{\mathrm{q}^2_{inlet}}{2g\mathrm{h}^2_M} - \mathrm{h}_M - B_M\right) h^2(x_{shock}) + \frac{\mathrm{q}^2_{inlet}}{2g} = 0, \\ h^3(x_{shock}) + \left(B(x_{shock}) - \frac{\mathrm{q}^2_{inlet}}{2g\mathrm{h}^2_{outlet}} - \mathrm{h}_{outlet}\right) h^2(x_{shock}) + \frac{\mathrm{q}^2_{inlet}}{2g} = 0, \\ \mathrm{q}^2_{inlet}\left(\frac{1}{h_1} - \frac{1}{h_2}\right) + \frac{g}{2}(h_1^2 - h_2^2) = 0 \end{aligned} \tag{54}$$

where h_1 and h_2 are the water depths upstream and downstream respectively. The position of the shock x_{shock} is located thanks to the third relation in system (54) which is known as

Rankine-Hugoniot's relation. The reader is referred to [36] to see the details. Numerical

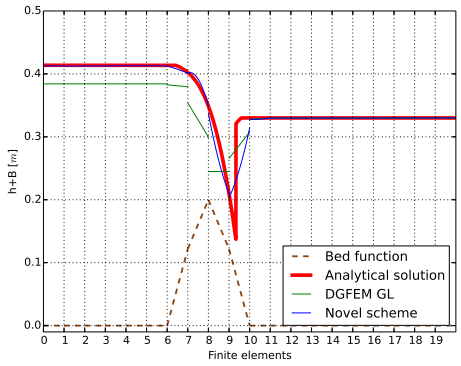

Figure 24: Water depth: transcritical flow with the shock.

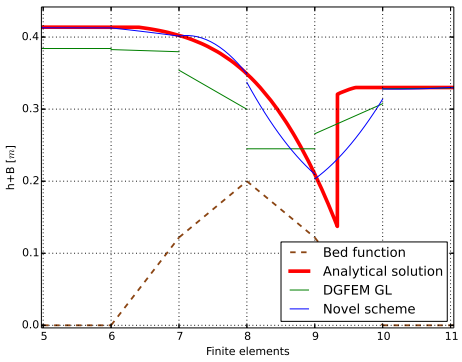

Figure 25: Detail of the water depth: transcritical flow with the shock.

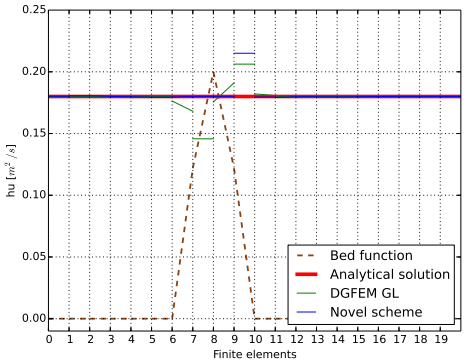

Figure 26: Discharge: transcritical flow with the shock.

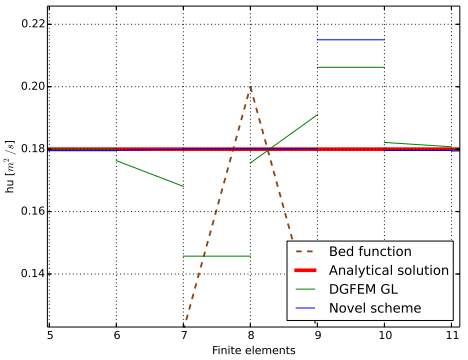

Figure 27: Detail of the discharge: transcritical flow with the shock.

solution of the water depth is shown in Figures 24 and 25. In Figures 26 and 27 the discharge is shown.

7 Conclusion

Novel limiting criterion for limiting process within discontinuous Galerkin method was introduced. This criterion works for both water depth and discharge variables. In Section

6.1 and 6.2, there was proven that this novel numerical scheme brings better accuracy than finite volume method and DGFEM with global limiting. In the paper there is also successfully implemented the wet/dry treatment used in the theory of finite volumes. This treatment ensures non-negativity of the water depth. Adopted velocity modification (39) avoids appearance of the non-physically large velocities caused by numerical inaccuracy.

It is concluded that the presented scheme is able to solve the flow over complex topography and keep the C-property in the flooded domain. The scheme also give good results for both wetting and drying processes.

The future work can be focused on the bed friction source term and its stability around wet/dry interface when the water depth is approaching zero values and wet/dry interface treatment for the bed function described by higher order polynomials.

Acknowledgment

References

[1] V.R. Ambati and O. Bokhove. Space–time discontinuous galerkin discretization of rotating shallow water equations. *Journal of Computational Physics*, 225(2):1233 – 1261, 2007.

[2] V.R. Ambati and O. Bokhove. Space–time discontinuous galerkin finite element method for shallow water flows. *Journal of Computational and Applied Mathematics*, 204(2):452 – 462, 2007. Special Issue: The Seventh International Conference on Mathematical and Numerical Aspects of Waves (WAVES'05).

[3] E. Audusse, F. Bouchut, M.O. Bristeau, R. Klein, and B. Perthame. A Fast and Stable Well-Balanced Scheme with Hydrostatic Reconstruction for Shallow Water Flows. *SIAM Journal on Scientific Computing*, 25(6):2050–2065, 2004.

[4] Emmanuel Audusse and Marie-Odile Bristeau. A well-balanced positivity preserving "second-order" scheme for shallow water flows on unstructured meshes. *Journal of Computational Physics*, 206(1):311–333, 2005.

[5] N. Beisiegel and J. Behrens. Quasi-nodal third-order bernstein polynomials in a discontinuous galerkin model for flooding and drying. *Environmental Earth Sciences*, 74(11):7275–7284, 2015.

[6] Andreas Bollermann, Guoxian Chen, Alexander Kurganov, and Sebastian Noelle. A well-balanced reconstruction of Wet/Dry fronts for the shallow water equations. *Journal of Scientific Computing*, 56:267–290, 2013.

[7] O. Bublík and A. Vimmr, J.and Jonášová. A local time step discontinuous galerkin finite element method for the solution of euler equations on unstructured meshes. *27th conference with international participation Computational Mechanics 2011*, pages 1–2, 2011.

[8] Ondřej Bublík, Jan Vimmr, and Alena Jonášová. Comparison of discontinuous galerkin time integration schemes for the solution of flow problems with deformable domains. *Applied Mathematics and Computation*, 267:329 – 340, 2015. The Fourth European Seminar on Computing (ESCO 2014).

[9] S. Bunya, E.J. Kubatko, J.J. Westerink, and C. Dawson. A wetting and drying treatment for the Runge–Kutta discontinuous Galerkin solution to the shallow wa-

ter equations. *Computer Methods in Applied Mechanics and Engineering*, 198(17-20):1548–1562, 2009.

[10] Vincenzo Casulli. A high-resolution wetting and drying algorithm for free-surface hydrodynamics. *International Journal for Numerical Methods in Fluids*, 60(4):391–408, 2009.

[11] D. Caviedes-Voullième, N. Gerhard, A. Sikstel, and S. Müller. Multiwavelet-based mesh adaptivity with Discontinuous Galerkin schemes: exploring 2D shallow water problems. *Advances in Water Resources*, 138:103559, 2020.

[12] D. Caviedes-Voullième and G. Kesserwani. Benchmarking a multiresolution discontinuous galerkin shallow water model: Implications for computational hydraulics. *Advances in Water Resources*, 86:14–31, 2015.

[13] B. Cockburn and C.W. Shu. Tvb runge-kutta local projection discontinuous galerkin finite element method for conservation laws ii: General framework. *Math. Comp.*, 52:411–435, 1989.

[14] O. Delestre, C. Lukas, P.A. Ksinant, F. Darboux, C. Laguerre, T.N.T. Vo, F. James, and S. Cordier. SWASHES: a compilation of shallow water analytic solutions for hydraulic and environmental studies. *International Journal for Numerical Methods in Fluids*, 72:269–300, 2013.

[15] I. Echeverribar, M. Morales-Hernández, P. Brufau, and P. García-Navarro. 2D numerical simulation of unsteady flows for large scale floods prediction in real time. *Advances in Water Resources*, 134:103444, 2019.

[16] M. Fišer, O. Bublík, L. Lobovský, and J. Vimmr. Problems and Solutions Connected with the Wet/Dry Interface in the Mathematical Model of the Shallow Water Equa-

tions. In *30th Conference with International Participation Computational Mechanics 2014*, pages 27–28, Špičák, 2014.

[17] Martin Fišer, Ilhan Özgen, Reinhard Hinkelmann, and Jan Vimmr. A mass conservative well-balanced reconstruction at wet/dry interfaces for the godunov-type shallow water model. *International Journal for Numerical Methods in Fluids*, 2016. fld.4246.

[18] David L. George. Adaptive finite volume methods with well-balanced Riemann solvers for modeling floods in rugged terrain: Application to the Malpasset dam-break flood (France, 1959). *International Journal for Numerical Methods in Fluids*, 66(8):1000–1018, 2011.

[19] A. Harten, P. Lax, and B. Leer. On Upstream Differencing and Godunov–Type Schemes for Hyperbolic Conservation Laws. *Society for Industrial and Applied Mathematics*, 25:35–61, 1983.

[20] F.M. Henderson. *Open channel flow*. Nordby, g. edn., Civil engineering, MacMillan, New York, 1966.

[21] J. Hou, Q. Liang, F. Simons, and R. Hinkelmann. A stable 2D unstructured shallow flow model for simulations of wetting and drying over rough terrains. *Computers & Fluids*, 82:132–147, 2013.

[22] J. Hou, F. Simons, Q. Liang, and R. Hinkelmann. An improved hydrostatic reconstruction method for shallow water model. *Journal of Hydraulic Research*, 52(June):1–8, 2014.

[23] J. Jaffre, C. Johnson, and A. Szepessy. Convergence of the discontinuous galerkin finite element method for hyperbolic conservation laws. *Mathematical Models and Methods in Applied Sciences*, 05(03):367–386, 1995.

[24] G. Kesserwani, J. Shaw, M. K. Sharifian, D. Bau, C. J. Keylock, P. D. Bates, and J. K. Ryan. (Multi)wavelets increase both accuracy and efficiency of standard Godunov-type hydrodynamic models. *Advances in Water Resources*, 129:31–55, 2019.

[25] Georges Kesserwani. Topography discretization techniques for Godunov-type shallow water numerical models: a comparative study. *Journal of Hydraulic Research*, 51(4):351–367, 2013.

[26] Georges Kesserwani and Qiuhua Liang. RKDG2 shallow-water solver on non-uniform grids with local time steps: Application to 1D and 2D hydrodynamics. *Applied Mathematical Modelling*, 39(3-4):1317–1340, 2015.

[27] L. Krivodonova, J. Xin, J.-F. Remacle, N. Chevaugeon, and J.E. Flaherty. Shock detection and limiting with discontinuous Galerkin methods for hyperbolic conservation laws. *Applied Numerical Mathematics*, 48(3-4):323–338, 2004.

[28] A. Kurganov and G. Petrova. A second-order well-balanced positivity preserving central-upwind scheme for the Saint-Venant system. *Communications in Mathematical Sciences*, 5(1):133–160, 2007.

[29] Alsar Lacasta, M Morales-Hernández, José Murillo, and Pilar García-Navarro. An optimized GPU implementation of a 2D free surface simulation model on unstructured meshes. *Advances in Engineering Software*, 78:1–15, 2014.

[30] Peter Lax. Weak solutions of nonlinear hyperbolic equations and their numerical computation. *Communications on Pure and Applied Mathematics*, 7:159–193, 1954.

[31] M.-S. Liou and C. Steffen. A new flux splitting scheme. *J. Comput. Phys.*, 107:23–39, 1993.

[32] Stephen C Medeiros and Scott C Hagen. Review of wetting and drying algorithms for numerical tidal flow models. *International Journal for Numerical Methods in Fluids*, 71(4):473–487, 2013.

[33] Claude Mügler, Olivier Planchon, J Patin, S Weill, Norbert Silvera, P Richard, and E. Mouche. Comparison of roughness models to simulate overland flow and tracer transport experiments under simulated rainfall at plot scale. *Journal of Hydrology*, 402(1-2):25–40, 2011.

[34] A. Navas-Montilla, P. Solán-Fustero, J. Murillo, and P. García-Navarro. Discontinuous Galerkin well-balanced schemes using augmented Riemann solvers with application to the shallow water equations. *Journal of Hydroinformatics*, in press:1–21, 2020.

[35] H. Nessyahu and E. Tadmor. Non-oscillatory Central Differencing for Hyperbolic Conservation Laws. *Journal of Computational Physics*, 87:408–463, 1990.

[36] S. Noelle, Y. Xing, and C. W. Shu. High-order well-balanced finite volume weno schemes for shallow water equation with moving water. *Journal of Computational Physics*, 226:29–58, 2007.

[37] J. Qiu and C.W. Shu. A comparison of troubled-cell indicators for runge–kutta discontinuous galerkin methods usingweighted essentially nonoscillatory limiters. *SIAM Journal on Scientific Computing*, 27:995–1013, 2005.

[38] W. Reed and T. Hill. Triangular mesh methods for the neutron transport equation. *Technical Report LA-UR-73-479, Los Alamos, NM, Los Alamos Scientific Laboratory*, 1973.

[39] P.L. Roe. Approximate Riemann solvers, parameter vectors and difference schemes. *Journal of Computational Physics*, 43:357–372, 1981.

[40] Franz Simons, Tobias Busse, Jingming Hou, Ilhan Özgen, and Reinhard Hinkelmann. A model for overland flow and associated processes within the Hydroinformatics Modelling System. *Journal of Hydroinformatics*, 16(2):375–391, 2014.

[41] J.J. Stoker. *Water waves*. Interscience Publishers, Wiley, New York, 1957.

[42] P.A. Tassi, O. Bokhove, and C.A. Vionnet. Space discontinuous galerkin method for shallow water flows—kinetic and {HLLC} flux, and potential vorticity generation. *Advances in Water Resources*, 30(4):998 – 1015, 2007.

[43] W.A. Thacker. Some exact solutions to the nonlinear shallow-water wave equations. *Journal of Fluid Mechanics*, 107:499–508, 1981.

[44] S. Vater, N. Beisiegel, and J. Behrens. A limiter-based well-balanced discontinuous Galerkin method for shallow-water flows with wetting and drying: Triangular grids. *International Journal for Numerical Methods in Fluids*, 91:395–418, 2019.

[45] Stefan Vater, Nicole Beisiegel, and Jörn Behrens. A limiter-based well-balanced discontinuous galerkin method for shallow-water flows with wetting and drying: One-dimensional case. *Advances in Water Resources*, 85:1 – 13, 2015.

[46] X. Xia and Q. Liang. A new efficient implicit scheme for discretising the stiff friction terms in the shallow water equations. *Advances in Water Resources*, 117:87–97, 2017.

[47] X. Xia, Q. Liang, and X. Ming. A full-scale fluvial flood modelling framework based on high-performance integrated hydrodynamic modelling system (HiPIMS). *Advances in Water Resources*, 132:103392, 2019.

[48] M. Yang and Z.J. Wang. A parameter-free generalized moment limiter for high-order methods on unstructured grids. *Advances in Applied Mathematics and Mechanics*, 1:451–480, 2009.

[49] J. Zhou, D.M. Causon, C.G. Mingham, and D. M. Ingram. The Surface Gradient Method for the Treatment of Source Terms in the Shallow-Water Equations. *Journal of Computational Physics*, 168(1):1–25, 2001.

[50] J. Česenek, M. Feistauer, and A. Kos. Dgfem for the analysis of airfoil vibrations induced by compressible flow. *ZAMM - Journal of Applied Mathematics and Mechanics*, 93:387–402, 2013.